Improving Fairness in Photovoltaic Curtailments via Daily Topology Reconfiguration for Voltage Control in Power Distribution Networks

Rahul K. Gupta and Daniel K. Molzahn

***Abstract*—In PV-rich power distribution systems, over-voltage issues are often addressed by curtailing excess generation from PV plants (in addition to reactive power control), raising fairness concerns. Existing fairness-aware control schemes tackle this problem by incorporating fairness objectives into the cost function. However, such schemes result in increased overall curtailments. This paper proposes a solution through daily topology reconfiguration, ensuring that different PV plants face varying grid conditions each day, leading to different curtailment levels and enhancing fairness. We illustrate that implementing this approach enhances overall fairness without significantly increasing overall curtailments. The optimization problem involves two stages. The day-ahead stage optimizes the network topology using day-ahead forecasts of PV generation and demand, minimizing net curtailment and accounting for fairness based on curtailments from prior days. The real-time stage implements the optimized topology and computes active and reactive power setpoints for the PV plants. Day-ahead grid constraints are modeled using linearized DistFlow equations, and real-time control employs a linearized model with a first-order Taylor approximation. The proposed scheme is numerically validated on several benchmark test cases including three-phase unbalanced distribution systems. Results are compared using the Jain Fairness Index, considering fairness and reconfiguration scenarios.**

***Index Terms*—Fairness, Feedback-based approach, Reconfiguration, Voltage control, Lin3DistFlow, PV curtailments.**

I. Introduction

Motivated by growing environmental concerns and financial incentives, there is a notable shift from traditional fossil-fuel-based power generation to renewable-based generation. This transition, often integrated into power distribution networks, presents significant operational challenges to the distribution grid [1]. Specifically, distribution system operators (DSOs) grapple with the task of managing the grid within operational voltage limits while adhering to the network's physical constraints [2]–[4]. The uncontrolled and uncoordinated integration of renewable-based generation sources poses particular challenges, giving rise to issues such as over-voltages, degradation of power quality, and congestion in lines and transformers [5]. These challenges become more pronounced when the net generation exceeds the demand, resulting in reverse power flow and causing over-voltages in the network. This phenomenon becomes a limiting factor for the hosting capacity of renewable sources in distribution systems.

A. Related work

On one hand, the literature addresses these challenges by advocating for the upgrade of the existing grid infrastructure through line and transformer reinforcements [6], grid expansion planning [7], tap-changing transformers [8], reactive var compensators [9], etc. In some cases, the installation of new distributed energy resources, such as battery energy storage systems, is also considered to mitigate this problem through energy shifting [10]. However, these solutions necessitate considerable investments and significant implementation times.

On the other hand, intelligent control and coordinated operation of PV plants can help mitigate operational problems caused by these resources, deferring the need for grid reinforcement, as highlighted in several recent works (e.g., [11]–[14]). Various studies propose leveraging the reactive power flexibility offered by PV inverters, often referred to as volt-var control schemes [11], [15]. However, this flexibility is constrained by the converter's apparent power capacity and operational bounds on the overall power factor [16]. In power distribution systems with high resistance-to-reactance ratios, reactive power control might be less effective than active power control, as shown in [17]. In such cases, recent literature suggests using active power curtailment (e.g., [18]–[21]) to address over-voltage issues. These schemes aim to minimize overall curtailment while considering grid operational constraints. They are implemented with a real-time control policy, where curtailment decisions are based on short-term forecasts of PV generation and grid constraints are accounted using power-flow models. In some cases, fixed generation limits are imposed on PV inverters to prevent over-voltage problems. For example, in [22], [23], a percentage of the DC power module is used as a generation limit. In [23], export limits are computed by formulating an optimal power flow (OPF) problem. However, as reported in [24], these active power curtailment actions often lead to unfairness among different PV owners due to different sensitivities between voltage fluctuations and power injections at different parts of the network. For instance, customers located at the end of the feeder are likely to face more curtailments compared to those near the substation.

Recently, researchers have increasingly studied fairness in the context of PV curtailments and proposed different fairness-aware control schemes [24]–[31]. These methods differ in how they enforce fairness in PV control algorithms. The work in [24] evaluates different objectives (maximize self-consumption, energy exported, and financial benefit) in terms of achieved fairness. The work in [25] proposes fair power curtailment by exploiting sensitivity matrix information in a P-V droop control scheme. In [26], an additional cost term is included in the curtailment minimization problem; this term reduces the variance of the curtailment across different PV plants. In [27], a fairness cost function is introduced, aiming to curtail proportionally to the energy exported. In [28], the

School of Electrical and Computer Engineering, Georgia Institute of Technology, Atlanta, GA, 30313, USA. Email: {rahul.gupta, molzahn}@gatech.edu. This work was supported by the Swiss National Science Foundation (SNSF), Postdoc Mobility under Grant 217874.

voltage-to-active-power sensitivity of the farthest PV plant is used as a parameter to achieve fairness in a volt-var-watt control scheme. In [29], a model-free control scheme is proposed, where fairness is accounted for by different objectives, one of which is fairness in curtailed PV proportionally to maximum available generation. In [30], a distributed optimization scheme is proposed, where fairness is also considered as an additional objective, proportionally curtailing PV generation. It also compares different cases, where fairness is observed with respect to individual PV plants compared to clusters of PV plants in different distributed areas. In [31], extra objectives minimize curtailment disparities among different PV owners using day-ahead PV generation and demand forecasts.

To summarize, most of the existing literature solves the fairness problem either by adding a fairness cost function in the optimization problem or by applying the same curtailments as the worst-curtailed PV plant using sensitivity information. These schemes work well in enhancing fairness in curtailments; however, they come at the cost of increasing the overall net curtailments, as reported in [30], [31]. In [31], it is shown that net curtailment doubles to improve fairness, quantified by the Jain Fairness Index (JFI) [32] from 0.3 to 1.0. A similar observation has been reported in [30].

We note that using a fairness function as an objective or constraint can lead to perverse outcomes where improving the value of the fairness function causes unnecessary curtailment, i.e., the fairness function can force some PV plants (probably those near the substation) to curtail despite not causing any voltage problems. In other words, increasingly curtailing some PV plants may improve a fairness function but not facilitate reduced curtailments of other PV plants. Thus, although more fair according to the selected fairness function, these actions result in an unnecessary overall loss of generation across all PV owners and are thus undesirable.

B. Proposed framework

The sensitivities of voltages to PV curtailments, and thus the optimal curtailments selected in many prior voltage control algorithms, is strongly related to PV plants' locations within the distribution network. While it is not possible to physically move the PV installations, their effective electrical locations can be implicitly controlled, to some extent, by reconfiguring the topology of the distribution network via actuating switches. Accordingly, in this work, we propose achieving fairness through the daily network reconfiguration of power distribution grids, ensuring that PV plants located at different positions encounter distinct grid conditions each day, resulting in varied curtailments. The daily reconfiguration aims to achieve fairness in PV curtailments cumulatively among different plants over the duration of a month. Fairness is considered by incorporating appropriate weight factors into the day-ahead objective function, determined based on curtailment decisions from previous days. The network reconfiguration process is repeated over several days, with weights updated daily based on the preceding days' curtailments. Our study shows that executing such topology configurations over an extended period (e.g., a month) can enable fairness in curtailment actions without significantly increasing overall curtailments.

We note that a conceptually similar network reconfiguration problem for achieving fairness in power outages due to wildfire risk mitigation is proposed in [33]. However, the approach in [33] only applies to the transmission systems, uses the DC power flow approximation, and considers deterministic single-period snapshots of extreme wildfire conditions without including solar PV generation. In contrast, the presented work applies to power distribution systems, uses the linearized DistFlow (LinDistFlow and Lin3DistFlow) equations, and focuses on stochastic multi-period solar PV during normal operations.

The proposed framework consists of two stages that aim to improve fairness across a specified period (e.g., monthly) using a feedback controller with both discrete and continuous actions. This framework is described below.

- **Day-ahead:** In this stage, we address the topology reconfiguration problem based on day-ahead forecasts of PV generation and demand, modeled as scenarios, and the realization of PV curtailments from previous days. We represent grid constraints using linearized grid models called LinDistFlow [34] and Lin3DistFlow [35] which are based on linearized approximations of the DistFlow model for single and three-phase systems, respectively, and neglect grid losses. The scheme incorporates radiality constraints as commonly used in distribution systems. The objective function aims to minimize overall curtailments for the next day's generation, weighted by "fairness weight factors" computed daily using prior days' curtailment realizations during real-time operation. The day-ahead problem is solved once a day.
- **Real-time:** In this stage, we utilize the network topology optimized in the day-ahead stage and solve the real-time voltage control problem during the day of operation. The real-time control problem is addressed every 15 minutes using short-term forecasts of PV generation and demand. The voltage control problem's objective minimizes total curtailments while satisfying the PV model and grid constraints, such as keeping nodal voltages within operational limits. The real-time control stage also incorporates weights derived from the day-ahead stage decisions to maintain consistency with the day-ahead formulation. Grid constraints are modeled using a linearized power-flow model [36], employing the first-order Taylor approximation of the original AC power flow model. These coefficients are based on the latest measurements of the operating point. Thanks to the linearized grid model, the formulation of the real-time control problem is linear.

The scheme is illustrated schematically in Fig. 1. The first part depicts the day-ahead optimization of the network topology and the second part represents real-time operation. The key contribution of this work is the development of a new scheme that enhances fairness in PV curtailments without substantially increasing net curtailments.

The paper is organized as follows: Section II describes the day-ahead reconfiguration problem, followed by Section III which presents the real-time control formulation. Section IV provides details on the numerical validation, and finally, Section V concludes the work.

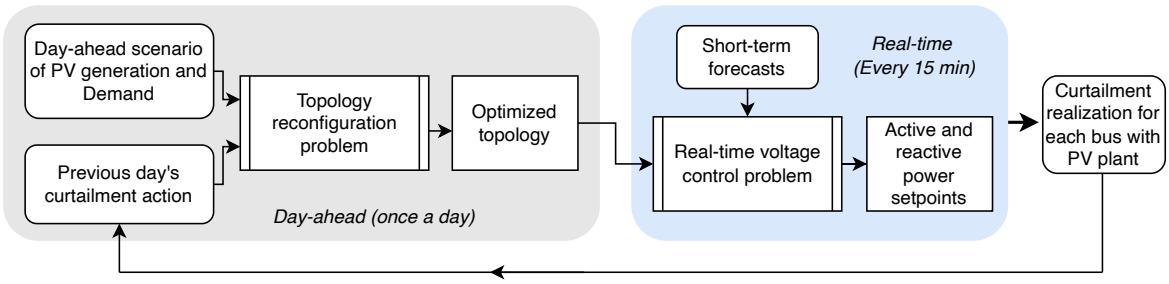

Fig. 1: Flow diagram of day-ahead and real-time operation. The day-ahead stage (left box) optimizes the network topology once a day. The real-time stage (right box) optimizes active and reactive power set-points of PV plants every 15-minutes.

TABLE I: Nomenclature

Symbols	Description
Ω	Set of Day-ahead scenarios
$\mathcal{T}$	Set of time-indices for a day
$\mathcal{L}$	Set of all the line indices
$\mathcal{L}_s$	Set of indices for lines with switches
$\mathcal{N}$	Set of non-slack bus indices
$\mathcal{N}_g$	Set of slack bus indices
$\mathcal{N}_{\text{pv}} \in \mathcal{N}$	Set of buses with PV plants
d_{kl}	On/off variable for line from k to l
$\bar{Z}_{lk} = R_{lk} + jX_{lk}$	Impedance for the line from l to k, $R_{lk} \in \mathbb{R}^{3\times3}$ and $X_{lk} \in \mathbb{R}^{3\times3}$ being the resistance and reactance
ξ_{kl}	Binary variable for switch in line between k to l
$S_{kl} = P_{kl} + jQ_{kl}$	Complex power flowing from bus k to l; $P_{kl} \in \mathbb{R}^{3\times1}$ and $Q_{kl} \in \mathbb{R}^{3\times1}$ are the active and reactive powers
$\mathfrak{L}_{kl} \in \mathbb{C}^{3\times1}$	Loss approximation for line from k to l with elements $\mathfrak{L}_{kl,\phi}$ for each phase ϕ
$\bar{I}_{lk} \in \mathbb{C}^{3\times1}$	Complex current flow in the line from l to k
$I_{lk}^{\max} \in \mathbb{R}^{3\times1}$	Ampacity for the line from l to k
$\bar{V}_l \in \mathbb{C}^{3\times1}$	Complex voltage at lth bus
$V^{\min}, V^{\max} \in \mathbb{R}^{3\times1}$	Voltage limits
$\Re(\cdot), \Im(\cdot)$	Real and imaginary operations
$P_{kl}^{\max}, Q_{kl}^{\max} \in \mathbb{R}^{3\times1}$	Bounds on active and reactive power flow for switching formulation of line k to l
$\mathfrak{M}$	Big-M number
$\hat{\bar{S}}^{\text{load}} = \hat{P}^{\text{load}} + j\hat{Q}^{\text{load}}$	Complex load forecast
$\bar{S}^{\text{pv}} = P^{\text{pv}} + jQ^{\text{pv}}$	Variable for complex PV power
$\bar{S}^{\text{inj}}$	Injection complex power
$\hat{P}^{\text{pv}}$	PV maximum power point potential
$S_{l,\max}^{\text{pv}}$	Converter capacity for the l-th PV plant

II. Day-ahead Topology Reconfiguration Problem

The day-ahead topology reconfiguration problem is solved every day using updated information on the forecasted PV generation and electricity demand obtained through day-ahead forecasting schemes, along with the realization of PV curtailments from the previous days. The optimization problem includes models of the PV plants, a grid model, and radiality constraints corresponding to the distribution system. In the following sections, we first describe these models and then present the day-ahead optimization problem. For the notation, we refer to the nomenclature listed in Table I.

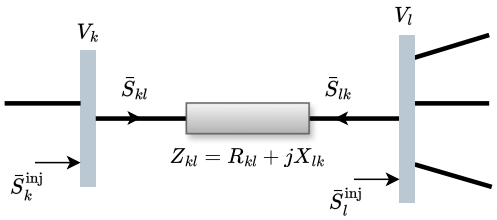

Fig. 2: Branch flow model in radial grids.

A. Power-flow constraints

1) Linearized DistFlow Model for three-phase unbalanced system (Lin3DistFlow model): In the day-ahead stage, we model grid constraints using the linearized DistFlow (Lin3DistFlow) model, derived from the branch-flow model known as the "DistFlow" equations, originally proposed in [34]. A schematic representation of the branch-flow model in radial grids is shown in Fig. 2. Using the notation in Table I, the DistFlow equations are:

$$V_k^2 = V_l^2 - 2\Re(\bar{S}_{lk}\bar{Z}_{kl}^*) + \bar{Z}_{kl}\bar{I}_{kl}\bar{I}_{kl}^*\bar{Z}_{kl}^*, \tag{1a}$$

$$\sum_{k:(l,k)\in\mathcal{L}} (\bar{S}_{kl} + \bar{Z}_{kl}\bar{I}_{kl}\bar{I}_{kl}^*) - \bar{S}_{lk} + \bar{S}_l^{\text{inj}} = 0, \tag{1b}$$

where $(.)^*$ is the complex conjugate of a complex quantity. LinDist3Flow, the linearized approximation of the DistFlow model, neglects the loss term $(\bar{I}_{kl}\bar{I}_{kl}^*)$ to obtain:

$$V_k^2 \approx V_l^2 - 2\Re(\bar{S}_{lk}\bar{Z}_{kl}^*) \tag{2a}$$

$$\sum_{k:(l,k)\in\mathcal{L}} \bar{S}_{kl} - \bar{S}_{lk} + \bar{S}_l^{\text{inj}} \approx 0. \tag{2b}$$

As illustrated in [35], the expression in (2a) is simplified as:

$$V_k^2 \approx V_l^2 + M_{lk}^P P_{lk} + M_{lk}^Q Q_{lk} \tag{2c}$$

where M_{lk}^P, M_{lk}^Q are defined using phase $\phi, \phi' \in \{a, b, c\}$ resistances $r_{\phi,\phi'}$ and reactances $x_{\phi,\phi'}$ as:

$$M_{lk}^P = \begin{bmatrix} -2r_{aa} & r_{ab} - \sqrt{3}x_{ab} & r_{ac} + \sqrt{3}x_{ac} \\ r_{ba} + \sqrt{3}x_{ba} & -2r_{bb} & r_{bc} - \sqrt{3}x_{bc} \\ r_{ca} - \sqrt{3}x_{ca} & r_{cb} - \sqrt{3}x_{cb} & -2r_{cc} \end{bmatrix}_{lk}, \tag{2d}$$

$$M_{lk}^Q = \begin{bmatrix} -2x_{aa} & x_{ab} + \sqrt{3}r_{ab} & x_{ac} - \sqrt{3}r_{ac} \\ x_{ba} - \sqrt{3}r_{ba} & -2x_{bb} & x_{bc} + \sqrt{3}r_{bc} \\ x_{ca} + \sqrt{3}r_{ca} & x_{cb} + \sqrt{3}r_{cb} & -2x_{cc} \end{bmatrix}_{lk}. \tag{2e}$$

2) Radiality constraints: Consistent with typical operational practices, we ensure radiality in the topology configuration problem. To this end, we employ radiality constraints from [37] as expressed in (3a)–(3e). These radiality constraints are based on the core idea that each node is supplied by a unique feeder station through a single path. This set of constraints ensure the absence of loops in the path connecting the substation and the loads. Loops without a substation cannot supply the loads, making them infeasible solutions.

The variables d_{kl} and d_{lk} are continuous; however, their optimized values are either 0 or 1, as proven in [37]. The formulation only requires binary variables ξ_{kl} for lines with switches as shown in (3c). The corresponding constraints are:

$$d_{kl} + d_{lk} = 1, \qquad \forall (l,k) \in \mathcal{L} \backslash \mathcal{L}_s, \tag{3a}$$
$$\sum_{kl \in \mathcal{L}} (d_{kl} + d_{lk}) = |\mathcal{N}| - 1, \qquad \forall (l,k) \in \mathcal{L} \backslash \mathcal{L}_s, \tag{3b}$$
$$d_{kl} + d_{lk} = \xi_{kl}, \quad \xi_{kl} \in \{0,1\}, \qquad \forall (l,k) \in \mathcal{L}_s, \tag{3c}$$
$$d_{kl} = 0, \qquad \forall l \in \mathcal{N}_g, \tag{3d}$$
$$\sum_{k:(l,k)\in\mathcal{L}} d_{kl} = 1, \qquad l \in \mathcal{N}. \tag{3e}$$

Using these radiality variables, the power flow bounds in both directions are modeled as:

$$-d_{kl} P_{kl}^{\max} \le P_{kl} \le d_{kl} P_{kl}^{\max}, \qquad \forall (l,k) \in \mathcal{L}, \tag{3f}$$
$$-d_{lk} P_{kl}^{\max} \le P_{lk} \le d_{lk} P_{lk}^{\max}, \qquad \forall (l,k) \in \mathcal{L}, \tag{3g}$$
$$-d_{kl} Q_{kl}^{\max} \le Q_{kl} \le d_{kl} Q_{kl}^{\max}, \qquad \forall (l,k) \in \mathcal{L}, \tag{3h}$$
$$-d_{kl} Q_{kl}^{\max} \le Q_{lk} \le d_{kl} Q_{kl}^{\max}, \qquad \forall (l,k) \in \mathcal{L}. \tag{3i}$$

The voltage constraints using the radiality variables and LinDist3Flow equations are modeled as:

$$V_k^2 \le V_l^2 + M_{lk}^P P_{lk} + M_{lk}^Q Q_{lk} + \mathfrak{M}(1 - d_{lk}), \quad \forall l \in \mathcal{N}, \tag{3j}$$
$$V_k^2 \ge V_l^2 + M_{lk}^P P_{lk} + M_{lk}^Q Q_{lk} - \mathfrak{M}(1 - d_{lk}), \quad \forall l \in \mathcal{N}, \tag{3k}$$
$$V_l^2 \le V_k^2 + M_{lk}^P P_{lk} + M_{lk}^Q Q_{lk} + \mathfrak{M}(1 - d_{kl}), \quad \forall l \in \mathcal{N}, \tag{3l}$$
$$V_l^2 \ge V_k^2 + M_{lk}^P P_{lk} + M_{lk}^Q Q_{lk} - \mathfrak{M}(1 - d_{kl}), \quad \forall l \in \mathcal{N}, \tag{3m}$$
$$(V^{\min})^2 \le V_l^2 \le (V^{\max})^2, \quad \forall l \in \mathcal{N} \backslash \mathcal{N}_g. \tag{3n}$$

The lines' apparent power flows are restricted by ampacity limits that are expressed as:

$$P_{kl}^2 + Q_{kl}^2 \le (V^{\min})^2 \odot (I_{lk}^{\max})^2, \qquad \forall (l,k) \in \mathcal{L}, \tag{3o}$$
$$P_{lk}^2 + Q_{lk}^2 \le (V^{\min})^2 \odot (I_{lk}^{\max})^2, \qquad \forall (l,k) \in \mathcal{L}. \tag{3p}$$

The final constraint approximates the line losses for the line from l to k by $\mathfrak{L}_{lk}$, which is then minimized in the objective in (5), it is

$$R_{kl}(P_{kl}^2 + P_{lk}^2 + Q_{kl}^2 + Q_{lk}^2) \le \mathfrak{L}_{lk}, \quad \forall (l,k) \in \mathcal{L}. \tag{3q}$$

B. PV as a controllable resource

For voltage regulation, we assume that PV plants are controllable, meaning their active power generation can be reduced from the available peak power (i.e., Maximum Power Point, MPP) and can accept reactive power setpoints within the converter capacity limits and power-factor constraints. Using the symbols for the active and reactive powers for PV plants as listed in Table I, let $p_{l,\phi}^{\text{pv}}(t,\omega)$ and $q_{l,\phi}^{\text{pv}}(t,\omega)$ are elements of P_l^{pv} and Q_l^{pv} denoting the active and reactive powers for the l-th PV plant for phase $\phi \in \{a,b,c\}$ at time t in scenario ω. The curtailability is defined by the following constraint that limits PV outputs between 0 kW and the MPP generation:

$$0 \le p_{l,\phi}^{\text{pv}}(t,\omega) \le \widehat{p}_{l,\phi}^{\text{pv}}(t,\omega), \quad \forall t \in \mathcal{T}, \omega \in \Omega, l \in \mathcal{N}_{\text{pv}}. \tag{4a}$$

The PV power plants can also inject/consume reactive power, which is limited by the power-factor constraint:

$$q_{l,\phi}^{\text{pv}}(t,\omega) \le p_{l,\phi}^{\text{pv}}(t,\omega)\zeta, \qquad \forall t \in \mathcal{T}, \omega \in \Omega, l \in \mathcal{N}_{\text{pv}}, \tag{4b}$$
$$-q_{l,\phi}^{\text{pv}}(t,\omega) \le p_{l,\phi}^{\text{pv}}(t,\omega)\zeta, \quad \forall t \in \mathcal{T}, \omega \in \Omega, l \in \mathcal{N}_{\text{pv}}, \tag{4c}$$

where $\zeta = \sqrt{(1 - \text{PF}_{\text{min}}^2)/\text{PF}_{\text{min}}^2}$ with PF_{min} denoting the minimum power factor allowed for the operation of each PV plant. For the sake of simplicity, we consider the same minimum power factor of 0.95 for all PV plants in the network.

The reactive power is also limited by the PV inverters' capacities restricting the apparent power to $s_{l,\text{max}}^{\text{pv}}$:

$$(p_{l,\phi}^{\text{pv}}(t,\omega))^2 + (q_{l,\phi}^{\text{pv}}(t,\omega))^2 \le (s_{l,\text{max}}^{\text{pv}})^2, \ \forall t \in \mathcal{T}, \omega \in \Omega, l \in \mathcal{N}_{\text{pv}}. \tag{4d}$$

The PV MPP $\left(\widehat{p}_{l,\phi}^{\text{pv}}(t,\omega)\right)$ in (4a) is modeled by a day-ahead forecasting scheme; more details on the forecasting model are provided in the numerical validation section (Sec. IV).

C. Day-ahead optimization problem

The objective function of the day-ahead optimization minimizes PV curtailment for all the PV plants while ensuring fairness in curtailment actions across different PV plants located at various locations in the network. The objective is:

$$f^{op}(\Theta, \xi, \mathbf{x}) = \sum_{l \in \mathcal{N}_{\text{pv}}} \sum_{\phi \in \{a,b,c\}} \lambda_l \Bigg\{ \sum_{\omega \in \Omega} \sum_{t} \left(\hat{p}_{l,\phi}^{\text{pv}}(t,\omega) - p_{l,\phi}^{\text{pv}}(t,\omega) \right) \Bigg\} + \sum_{(i,j) \in \mathcal{L}} \sum_{\omega \in \Omega} \sum_{\phi \in \{a,b,c\}} \sum_{t} (\mathfrak{L}_{ij,\phi}(t,\omega)), \tag{5}$$

where $\mathbf{x} = [P_{kl}, Q_{kl}, d_{kl}, p_{l,\phi}^{\text{pv}}(t,\omega), \forall j, \omega, \phi]$ collects the continuous variables, $\xi = [\xi_{kl}, \forall (l,k) \in \mathcal{L}_s]$ collects the binary variables, and $\Theta = [\hat{p}_{l,\phi}^{\text{pv}}(t,\omega), \forall j, \omega, \phi]$ refers to parameters.

The symbol λ_l refers to the weights which are used to achieve fairness in curtailments. As we will discuss next, the weights are determined using realizations of the real-time control from previous days. We compute the cumulative normalized generation for each PV plant for D days of realization as $\mathcal{G}(P_l^{\text{pv}}, \hat{P}_l^{\text{pv}}, D) =$

$$\mathcal{G}_l^{1 \to D} = \frac{\sum_{\phi \in \{a,b,c\}} \sum_{d=1}^{D} \sum_{t \in \mathcal{T}} p_{l,\phi}^{\text{pv}}(t,d)}{\sum_{\phi \in \{a,b,c\}} \sum_{d=1}^{D} \sum_{t \in \mathcal{T}} \hat{p}_{l,\phi}^{\text{pv}}(t,d)}, \tag{6}$$

where $p_{l,\phi}^{\text{pv}}(t,d)$ refers to decisions for d-th day.

Each weight coefficient is computed as the inverse of $\mathcal{G}_l^{1 \to D}$ to penalize further curtailments of the PV plants that had significant previous curtailment:

$$\lambda_l = 1/\mathcal{G}_l^{1 \to D}. \tag{7}$$

Other choices for weight coefficients can also be employed with similar but distinct effects. The numerical results in Section IV analyze different choices for the weights via their outcomes in terms of fairness and overall curtailment.

The day-ahead reconfiguration problem is formulated as

$$\underset{\mathbf{x},\xi}{\text{minimize}}\ f^{op}(\Theta,\xi,\mathbf{x}) \tag{8a}$$

$$\text{subject to: (2b), (3), (4).} \tag{8b}$$

In the nodal power balance constraint (2b), power injections are related to the load forecasts and PV active and reactive generation variables as $\bar{S}_l^{\text{inj}} = \hat{\bar{S}}_l^{\text{load}} - \bar{S}_l^{\text{pv}}, \forall l \in \mathcal{N}_{\text{pv}}$ else $\bar{S}_l^{\text{inj}} = \hat{\bar{S}}_l^{\text{load}}, \forall l \in \mathcal{N}\backslash\mathcal{N}_{\text{pv}}$. Eqs. (2b), (3) includes constraints for each timestep $t \in \mathcal{T}$ and scenario $\omega \in \Omega$.

Note that the objective in (8) does not consider an additional fairness objective, as is common in prior literature (e.g., [31]); rather, fairness is accounted for by the weights λ_l. Such a scheme helps avoid unnecessary curtailment for the sake of increasing fairness as will be demonstrated later in Sec. IV-C. The problem in (8) is a mixed-integer program with convex-quadratic constraints (MIQCP) and can be effectively solved by off-the-shelf solvers (e.g., Gurobi).

III. Real-time Voltage Control Problem

The real-time stage implements the voltage control problem, considering the optimized topology from the day-ahead stage, as shown in Fig. 1. Real-time control aims to optimize the active and reactive power setpoints for the PV inverters, ensuring that nodal voltages during real-time operation are respected. The real-time control stage is based on short-term forecasts of the PV generation and load demand. The linearized DistFlow model used to represent grid constraints in the day-ahead stage can suffer from inaccuracies due to neglecting the $\bar{Z}_{kl}\bar{I}_{kl}\bar{I}_{kl}^*$ term in (2a). Conversely, with access to more accurate short-term forecasts, the real-time stage models voltage constraints via a linearization of the AC power-flow model based on the first-order Taylor approximation and is given as:

$$\begin{aligned} V_m(t) =& \tilde{V}_m(t-1) + \sum_{l\in\mathcal{N}^{\text{pv}}} \Big\{ K_{ml}^P(t-1)\Big(P_l^{\text{pv}}(t) - \tilde{P}_l^{\text{pv}}(t-1)\Big) + \\ &+ K_{ml}^q(t-1)\Big(Q_l^{\text{pv}}(t) - \tilde{Q}_l^{\text{pv}}(t-1)\Big)\Big\} \quad \forall m \in \mathcal{N}, \end{aligned} \tag{9}$$

where P_l^{pv} and Q_l^{pv} stacks PV's active and reactive power for all the phases for node l. The coefficients $K_{ml}^p(t-1)$ and $K_{ml}^q(t-1)$ are the voltage magnitude sensitivity coefficients for node m with respect to the active and reactive power injections at node l at time index $(t-1)$. These coefficients are determined through linearization at each time-step, which is solved using the method described in [36], [38]. In this context, the coefficients are computed based on information about voltage magnitudes $\widehat{V}_m(t-1)$ and power measurements $\tilde{P}_l^{\text{pv}}(t-1)$ and $\tilde{Q}_l^{\text{pv}}(t-1)$ at time $(t-1)$, along with the compound admittance matrix of the network.

The real-time scheme uses the same objective function as in the day-ahead stage (except the loss term). The real-time problem is formulated for each time t as

$$\text{minimize} \sum_{l\in\mathcal{N}^{\text{pv}}} \lambda_l \times (\hat{P}_l^{\text{pv}}(t) - P_l^{\text{pv}}(t)) \tag{10a}$$

$$\text{subject to: PV constraints for time } t\text{ : (4)}, \tag{10b}$$

$$V^{min} \le V_m(t) \le V^{max}, \quad \forall m. \tag{10c}$$

The weight λ_l is the same as in (7). This real-time voltage control problem is solved every 15 minutes, utilizing updated information on the PV generation forecast $(\hat{P}_l^{\text{pv}}(t))$ and information on the grid state from the previous time step. Once the setpoints of the active and reactive powers are computed, they are implemented on the inverters and serve as inputs for the optimization of the next time step. This process is repeated throughout the day.

IV. Numerical Validation

We validate the proposed scheme on several distribution test cases. First, results are presented for the unbalanced three-phase `ieee37` system. We then validate the proposed fairness scheme on other test cases such as `case33` [34], `case69` [34], `case123` [39], `case141` [40], `case533` [41]. We next present a comparison of the proposed scheme with respect to the fixed topology when fairness is enforced by an extra objective. We also present a sensitivity analysis with different weighing policies λ_l that are used in the objective function (5).

A. IEEE37 benchmark test case

1) Setup: The `ieee37` test case is shown in Fig 3; the test-case is modified by additional lines that can be switched, and we have also converted some of the existing lines as switchable. The modified test-case contains 16 lines to be switchable as marked with a dotted line in Fig 3. We assume to have the active and reactive loads of 150 kW and 70 kVar at all the nodes and as well install PV plants at nodes of the nominal rating of 330 kWp at each node except at nodes 799, 701, and 744. For the simulation, we do not consider the possibility of phase swapping or switching.

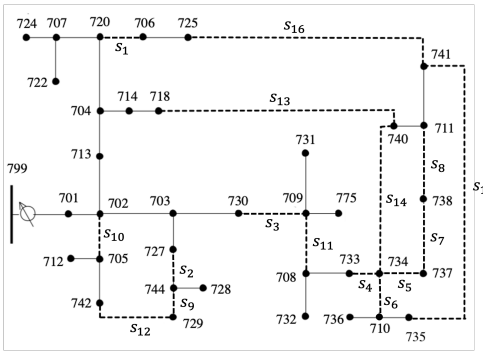

Fig. 3: Modified `ieee37` unbalanced three-phase network with dashed lines that are considered switchable.

The simulation spans 30 days to demonstrate the cumulative benefits of daily reconfiguration in terms of increasing fairness and decreasing net curtailments. For each day's simulation, we follow the operational flow illustrated in Fig. 1. The day-ahead stage solves (8) a few hours before the day of operation to determine the optimal topology for the next day based on forecasts of PV generation and load. This stage also takes as input the curtailment realizations from the previous days' operation, if available. If these curtailment decisions from previous days are not available (e.g., on the first day of day-ahead optimization), it is assumed that there was no curtailment. These curtailment actions are then used to

compute the weights λ_l using the fairness function as defined in (7). On the day of operation, the optimized topology from the day-ahead solution is utilized for real-time control by solving (10) every 15 minutes.

2) Day-ahead and intraday-forecasts: We next describe the day-ahead and short-term forecasting schemes for PV generation and demand, which serve as inputs for the day-ahead and real-time optimization stages.

a) Day-ahead scenarios: For PV generation, we leverage the commercial Solcast service [42], which provides Global Horizontal Irradiance (GHI) and air temperature forecasts for the next day at a time resolution of 15 minutes. This data is then used to estimate PV generation, considering information on PV panel capacity, tilt, and orientation (assumed to be known to the modeler), utilizing the PV-lib model [43].

For the load, we employ a previously developed forecasting model described by Algorithm 1 in [44]. This model utilizes a multi-variate Gaussian approach with historical time-series data of the demand. The model is constructed by clustering historical measurements into different day types based on the days of the week. For each cluster, a multivariate distribution is trained, considering time correlations, and is then used to sample new scenarios. This trained model is applied to generate scenarios for the day-ahead optimization.

For numerical validation, we model day-ahead uncertainties by considering two extreme scenarios: associating the lower PV scenario with a higher load scenario and vice versa. However, it is important to note that the proposed formulation is generic enough to account for any number of scenarios.

b) Short-term forecast: Short-term PV generation forecasts are essential for real-time operation to model the PV generation potential. The real-time scheme requires the MPP forecast of the PV generators for the next time-step, which is utilized in the constraint (4a). We assume that GHI measurements are available through an experimental setup, for example, one similar to those described in [44]. These GHI and air-temperature measurements are then used to compute the short-term MPP forecast for PV generation units, as similarly described for the day-ahead forecast.

A short-term load forecast is needed to compute the power-flow linearization, which requires a nominal operating point as described in [45]. Here, we assume access to measurements of voltage and power injections from the previous time-step, which are used as the operating point for linearization. In the numerical simulation, we employ the solutions of the real-time voltage control from the previous time step as measurements.

3) Numerical results: We present results for two different cases. First, we simulate a case where we assume the same PV generation and load scenarios every day for 30 days. This simulation is conducted to analyze the benefit of topology configuration without the influence of uncertainty caused by PV generation and load. This case is referred to as the "Similar days" scenario, and the results are presented in Sec. IV-A3a. In the second case, we simulate a "varying days" scenario where we account for the daily variation in the load and PV using real data. The results for this case are presented in Sec. IV-A3b.

a) Similar days scenario: Same PV and load scenarios for each day: We first use the same PV generation and load day-ahead forecasts and realizations (the ones depicted in Fig. 4) for the next 30 days. Scenarios 1 and 2 are employed in the day-ahead formulation, while the realization shown in orange is used for real-time control. These values are presented in per unit (of the nominal rating per node, i.e., 150 kW / 70 kVar for loads and 330 kWp for PV plants) and are used to compute the profiles per node by multiplying with the nominal values indicated in the test case shown in Fig. 11.

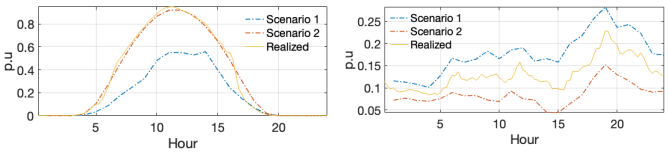

(a) PV generation potential (MPP) scenarios and realization.

(b) Active demand scenarios and realization.

Fig. 4: Day-ahead scenarios and realization for (a) PV generation and (b) load for similar days scenario. These scenarios are multiplied with the nominal active/reactive demand and PV generation capacities to obtain nodal demand and generation per node.

The simulation results are presented in Figs. 5–6. To quantify fairness, we utilize Jain's Fairness Index (JFI) [32], a metric designed to quantify the spread of benefits to each consumer using different control schemes. JFI values range between 0 and 1, where JFI = 0 and JFI = 1 refer to completely unfair and fair cases, respectively. Regarding fairness in generation at different PV plants, the JFI is

$$\text{JFI}^{1\to D} = \frac{(\sum_{l\in\mathcal{N}_{\text{pv}}} \mathcal{G}_l^{1\to D})^2}{|\mathcal{N}_{\text{pv}}|\sum_{l\in\mathcal{N}_{\text{pv}}} (\mathcal{G}_l^{1\to D})^2}, \tag{11}$$

where $\mathcal{G}_l^{1\to D}$ refers to the percentage of PV energy produced using (6). In the results, we also show per-day JFI, denoted as $\text{JFI}^{(D-1)\to D}$ computed using $\mathcal{G}_l^{(D-1)\to D}$.

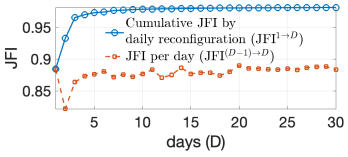

(a) Cumulative Jain Fairness Index (in blue) and per day (in red).

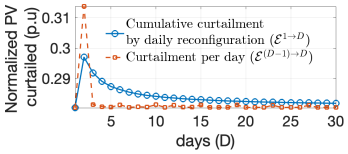

(b) Cumulative normalized PV curtailments (in blue) and per day curtailments (in red).

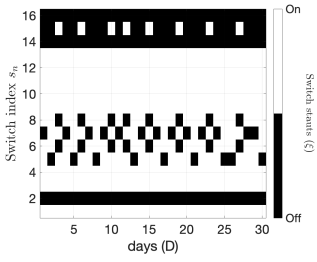

(c) Line status per day: black represents open lines, and white represents closed lines.

Fig. 5: (a) Jain Fairness Index, (b) Net PV curtailments, and (c) Switch status for 30 days of simulation of the "similar days" scenario.

Fig. 5a shows the cumulative JFI ($\text{JFI}^{1\to D}$) as a result of network reconfiguration each day and JFI computed per day $\text{JFI}^{(D-1)\to D}$ of operation in blue and red color, respectively. Observe that the cumulative JFI increases through the simulation period of the whole month, whereas JFI per day is always lower than the cumulative JFI.

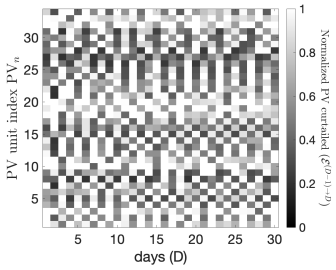

(a) Per day normalized PV curtailments ($\mathcal{E}_l^{1\to D}$) for different PV units.

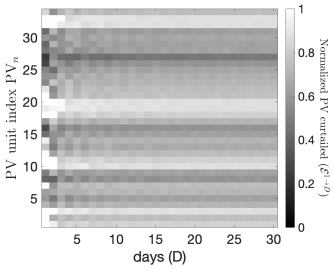

(b) Cumulative normalized curtailments ($\mathcal{E}_l^{(D-1)\to D}$) for different PV units.

Fig. 6: Normalized PV curtailments for different PV plants per day for the "similar days" scenario.

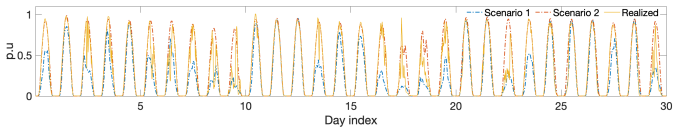

(a) PV generation potential (MPP) scenarios and realization for 30 days.

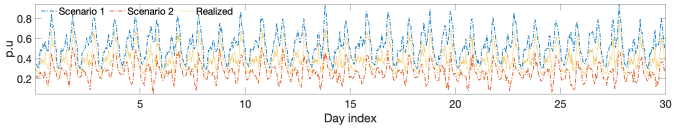

(b) Active demand scenarios and realization for 30 days.

Fig. 7: Day-ahead scenarios and realization for (a) PV generation and (b) load for the varying days scenario. These scenarios are multiplied with the nominal active/reactive demand and PV generation capacities to obtain nodal demand and generation per node.

We also present the normalized curtailed PV (relative to the MPP generation potential) in Fig. 5b, which shows the cumulative curtailments $\mathcal{E}_l^{1\to D} = 1 - \mathcal{G}_l^{1\to D}$ and curtailments per day $\mathcal{E}_l^{(D-1)\to D} = 1 - \mathcal{G}_l^{(D-1)\to D}$. Net curtailments decrease gradually after an initial increase on the second day. This initial increase can be attributed to the choice of a topology that penalizes PV plants not curtailed on the first day, resulting in a peak in the JFI index on the second day. In contrast, the daily curtailments exhibit fluctuations along the cumulative curtailment curve, indicating that different topologies lead to varying amounts of net curtailments. This suggests that the proposed algorithm dynamically switches between different topologies to enhance fairness overall.

The line switching decisions are depicted in Fig. 5c. Each column represents the switching configuration for a specific day. For instance, on day 1, switches s_2, s_7, s_{14}, s_{15}, and s_{16} are off, and on day 2, s_7 and s_5 turn on and off, respectively, and so forth. The topology varies between three different configurations throughout the month. Observing the plots of PV curtailment and JFI per day, we see that one configuration may result in higher curtailment and lower JFI than another. However, due to the switching over the month, the overall cumulative curtailment decreases, and JFI improves simultaneously. We also present the evolution of PV curtailment per day in Figs. 6a and 6b for each day and cumulatively, respectively. There is a substantial change in the curtailment patterns across PV plants each day, reflecting the impact of topology changes shown in Fig. 5c. These topology changes contribute to the settling of cumulative curtailments for each PV plant, as depicted in Fig. 6b.

Furthermore, Table II provides a comparison of JFI and PV curtailment between fixed and daily configuration cases. It is evident that the daily reconfiguration scheme enhances fairness by 10% while worsening PV curtailments by only 1%.

Overall, for this simulated deterministic case, topology reconfiguration demonstrates an increase in fairness, as quantified by JFI with almost no increase in net curtailment. This is quite significant; alternative approaches such as formulations that impose extra fairness costs in the objective (e.g., [31]) usually lead to much larger increases in PV curtailments. A detailed comparative analysis is presented in Sec. IV-C. In the next section, we present the results for the varying days scenario with daily load and PV generation forecast updates.

TABLE II: With and Without Daily Reconfiguration for the Similar Days Scenario.

Fairness schemes	JFI	PV curtailed
Without daily reconfiguration	0.88	0.28
With daily reconfiguration (proposed)	**0.99**	**0.29**

b) Varying days scenario: Varying PV generation and demand per day: This case is simulated with real PV and load generation profiles, which are updated each day using the forecasting model described in Sec. IV-A2a. Fig. 7a and 7b show the day-ahead PV and demand forecast for each day, respectively, along with the realized PV and load for each day. For the PV, realized PV generation is derived from real GHI measurements using the experimental setup from [36]. For the load realization, we use the mean of the day-ahead scenarios due to the lack of real measurements.

The simulation results for this case are shown in Figs. 8–6. Figs. 8a and 8a again display JFI and PV curtailments (cumulatively and per day), respectively. Fig. 8c illustrates the switching decisions. Finally, Figs. 9a and 9b present the distribution of curtailments per PV generator per day, individually and cumulatively. As observed, the results differ slightly from the "similar days" scenario due to the influence of changing generation and load conditions each day.

Comparing the JFI results between Fig. 5a and 8a, we observe again that JFI per day is always lower than in the reconfiguration case. However, in contrast to the "similar days" scenario simulations, we observe that the curtailments are sometimes higher than the one with reconfiguration in the "varying days" scenario, as shown in Fig. 8a. We again show the curtailments per PV plant for the period of 30 days in Figs. 9a and 9b. Comparing these two figures, shows that we achieve close to uniform curtailments (evident from similar colors in each column of Fig. 9b) in the case with reconfiguration, whereas without reconfiguration there is substantial disparities in the curtailments (evident from quite distinct colors in each column of Fig. 9b).

Comparing the switching decisions for the two cases in Fig. 5c and 8c reveals that every day except the few days have same set of topologies, suggesting that a small set of topologies suffices for improving fairness. Overall, we observe

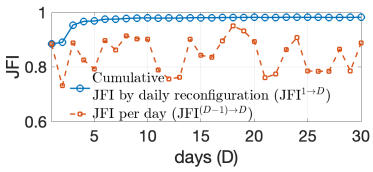

(a) Cumulative Jain Fairness Index (in blue) and per day (in red).

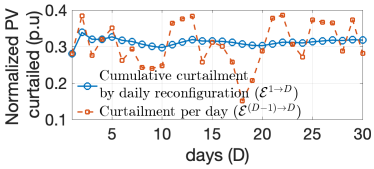

(b) Cumulative normalized PV curtailments (in blue) and per-day curtailments (in red).

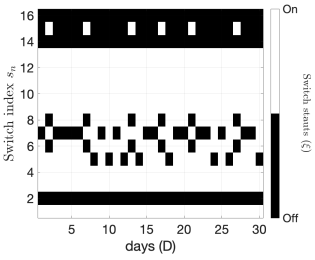

(c) Line status per day: black represents open lines, and white represents closed lines.

Fig. 8: (a) Jain Fairness Index (b) Net PV curtailments and (c) Switch status for 30 days of simulation for the "varying days" scenario.

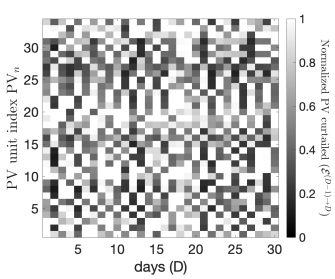

(a) Per-day normalized PV curtailments ($\mathcal{E}_l^{1\to D}$) for different PV units.

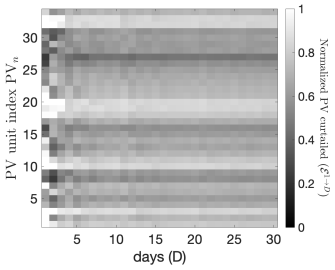

(b) Cumulative normalized curtailments ($\mathcal{E}_l^{(D-1)\to D}$) for different PV units.

Fig. 9: Normalized PV curtailments for different PV plants per day for the "varying days" scenario.

an increase in JFI, like the "similar days" scenario case, thanks to the proposed daily reconfiguration scheme.

B. Validation for other benchmark test cases

We also validate the proposed algorithm for several other test networks: `case33` [34], `case69` [34], `case123` [39], `case141` [40], and `case533` [41] systems, with the results given in Table III. We present the comparison between the cases with and without daily reconfiguration schemes. Here, we show the results considering the "similar days" scenario. As shown in the table, the daily reconfiguration scheme achieves substantially better fairness outcomes for all test cases compared to the base case with no reconfiguration, with minimal impacts on overall curtailments.

We also show the computation time for the reconfiguration schemes in Table IV. As the number of lines and size of the network increase, we see an increase in the computation time.

TABLE III: With and without daily reconfiguration (other test cases).

	Fixed topology		Daily reconfiguration	
Case	**JFI**	**PV curtailed**	**JFI**	**PV curtailed**
`case33`	0.83	0.28	**0.90**	0.30
`case69`	0.89	0.28	**0.95**	0.30
`case123`	0.88	0.21	**0.97**	0.22
`case141`	0.77	0.33	**0.91**	0.34
`case533`	0.87	0.12	**0.93**	0.13

TABLE IV: Computation time (sec)

`ieee37` $\lvert\mathcal{L}_s\rvert = 16$	`case33` = 13	`case69` = 21	`case123` = 19	`case141` = 21	`case533` = 76
117	4.2	14.6	204.8	64.2	12484

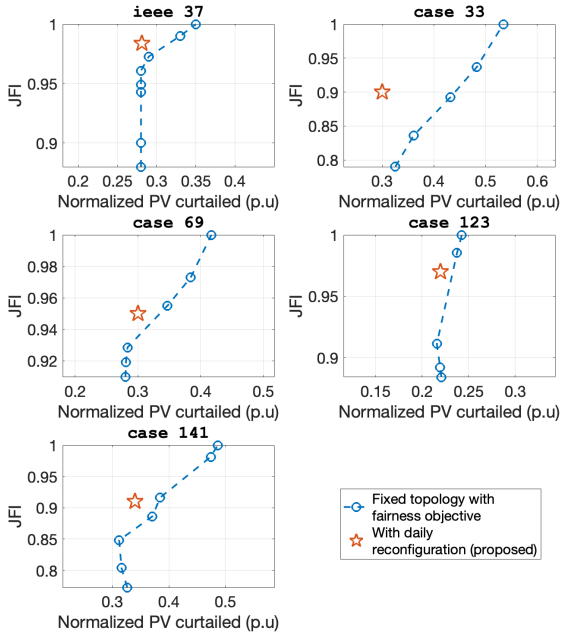

Fig. 10: Comparisons of the *proposed* daily reconfiguration against the fixed topology case with fairness enforced by an extra objective.

C. Comparison with Fixed Topology where Fairness is Modeled via an Augmented Objective

We also compare the performance of the proposed scheme with an alternative approach, which uses a fixed topology and enforces fairness by adding an *extra fairness term* to the objective, as described in [31]. Additionally, a fixed topology is imposed in the reconfiguration problem. In this case, the objective function in (5) is modified as $g^{op}(\Theta, \xi, \mathbf{x}) =$

$$f^{op}(\Theta, \xi, \mathbf{x}) + \alpha \sum_{\omega \in \Omega} \left| \gamma_\omega - \frac{\sum_{\omega \in \Omega} \sum_t \sum_{\phi \in \{a,b,c\}} p^{\text{pv}}_{l,\phi}(t,\omega)}{\sum_{\omega \in \Omega} \sum_t \sum_{\phi \in \{a,b,c\}} \hat{p}^{\text{pv}}_{l,\phi}(t,\omega)} \right| \quad (12)$$

where γ_ω is a common metric (per scenario) that enforces fairness among different PV plants.

We perform the comparison by varying the weight α in the objective (12), yielding the plot in Fig. 10. The blue curve is obtained by varying α in (12). A small and larger value of α leads to the point on the lower left (with low JFI) and and point on the upper right (high JFI), respectively. The JFI and PV curtailment achieved by the proposed reconfiguration scheme is shown in red star point. For all the networks, we observe the proposed scheme performs better in terms of JFI for the same amount of PV curtailment. This suggests that schemes which augment objectives with fairness terms can lead to unnecessary curtailment and sub-optimal solutions, whereas the proposed scheme always performs better in terms of JFI for the same amount of PV curtailment.

D. Sensitivity with different weighting policies

We also perform analyses with different weight policies. In (7), the weight λ is chosen as the inverse of normalized PV generation $\mathcal{G}^{1\to D}$, which is defined using the curtailment actions that occurred from day $d = 1$ to the current day D. Such weights lead to a sharp increase in JFI after the first day of operation, as observed in Figs. 5 and 8. In this section, we explore different weighting policies that can reduce this sharp increase in JFI. The results are presented for the `case33` network shown in Fig. 11 augmented with many PV units (to create over-voltages such that voltage control is required).

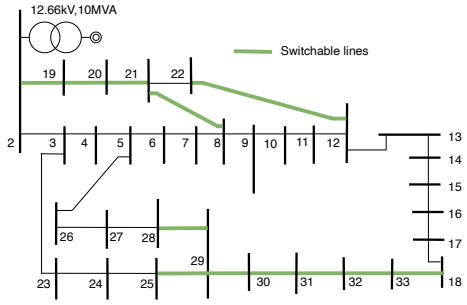

Fig. 11: `case33` from [34] augmented with several PV plants; lines highlighted in green are switchable.

1) Shrinking and rolling horizon policies: Since the objective is to achieve fairness by the end of month operation, one can delay the fairness action by modifying the weights:

$$\lambda_l^{1\to D\dashrightarrow 30} = \frac{\sum_{\phi\in\{a,b,c\}}\sum_{t\in\mathcal{T}}\left(\sum_{d=1}^{D}\hat{p}^{\text{pv}}_{l,\phi}(t,d)+\sum_{d=D+1}^{30}\hat{p}^{\text{pv}}_{l,\phi}(t,d)\right)}{\sum_{\phi\in\{a,b,c\}}\sum_{t\in\mathcal{T}}\left(\sum_{d=1}^{D}p^{\text{pv}}_{l,\phi}(t,d)+\sum_{d=D+1}^{30}\hat{p}^{\text{pv}}_{l,\phi}(t,d)\right)}. \tag{13}$$

In this way, the weights account not only for realizations from previous days but also for future realizations based on their forecasts. For our numerical analysis, we assume that there are no curtailments in the upcoming days, and the generation will be similar to the current day.

A variation of this policy is the *rolling horizon policy*, where λ_l is computed based on the forecast for R upcoming days instead of considering the entire month. In this case, $\lambda_l^{1\to D\dashrightarrow R}$ is used for $R \le D$, and $\lambda_l^{1\to D\dashrightarrow 30}$ for $R > D$.

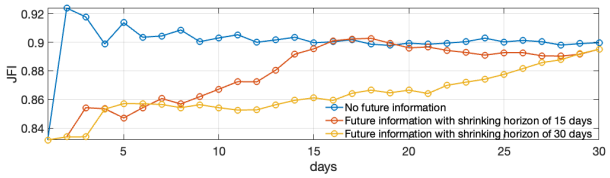

(a) Cumulative Jain Fairness Index for 30 days of simulation.

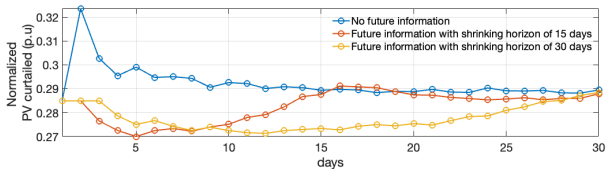

(b) Cumulative PV curtailments for 30 days of simulation.

Fig. 12: Fairness and normalized PV curtailments for the deterministic case with shrinking and rolling horizon policies.

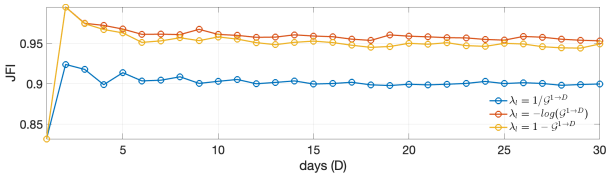

(a) Cumulative Jain Fairness Index for 30 days of simulation.

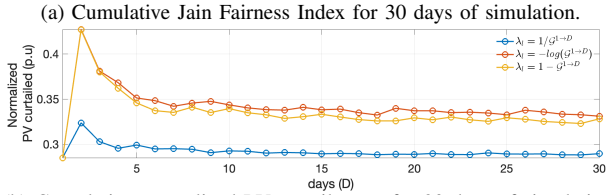

(b) Cumulative normalized PV curtailments for 30 days of simulation.

Fig. 13: Fairness and normalized PV curtailments for the similar days scenario with different weight functions.

We compare the results for this case in Fig. 12. As depicted in Fig. 12a, the JFI index increases smoothly with a shrinking policy of 30 days and 15 days, respectively, compared to the base case. The curve with a shrinking policy of 15 days reaches its peak in the middle and then settles. Note that all three cases converge to the same JFI value. The same behavior is also observed for curtailed PV in Fig. 12b.

2) Other weight functions: We also assess other options that could provide stronger penalties to the curtailments objectives compared to (7). The first is *Logarithmic* which is given as $\lambda_l = -\log(\mathcal{G}_l^{1\to D})$ and second one is *Difference* which is given as $\lambda_l = 1 - \mathcal{G}_l^{1\to D}$. We compare results in Fig. 13. As observed, the JFI is higher in the cases of "logarithmic" and "difference" compared to the base case of (7); however, these also result in higher PV curtailments.

V. Conclusions

In this paper, we present a framework for enhancing fairness regarding PV curtailment in power distribution grids. The framework comprises two stages. In the first stage, daily network topology reconfiguration is carried out, where fairness is achieved by weighting the curtailment minimization problem, penalizing PV plants that were not curtailed previously. This weighting policy results in a reconfigured network that favors PV plants that were curtailed before. In the second stage, the optimized topology is implemented along with the voltage control scheme. We utilized a Linearized Distflow model for the first stage and a first-order Taylor approximation of the AC power flow equations for the second stage.

Our numerical validation on several benchmark test networks showed better performance of the proposed framework in terms of increasing fairness while avoiding significant curtailments compared to the base case when no network topology reconfiguration was performed.

We also conducted sensitivity analyses with different weight policies. Weight policies that account for future information of the PV generation by forecasts reduced the sharp increase in JFI and PV curtailments in the early time periods. Weight policies based on logarithmic and difference functions resulted in higher JFI at the cost of increased PV curtailments.

Future work will investigate the optimal placement of the switches in the power distribution network to best enable fairness in photovoltaic curtailments under the proposed scheme.

ACKNOWLEDGEMENT

The authors gratefully acknowledge the support of Prof. Mario Paolone, Head of the Distributed Electrical Systems Laboratory, EPFL, Switzerland for providing the data that are used in this paper.

REFERENCES

[1] S. M. Ismael, S. H. A. Aleem, A. Y. Abdelaziz, and A. F. Zobaa, "State-of-the-art of hosting capacity in modern power systems with distributed generation," *Renewable Energy*, vol. 130, pp. 1002–1020, 2019.

[2] Power Quality Application Guide, "Voltage disturbances," *Standard EN*, vol. 50160, 2004.

[3] CIGRE Task Force C6.04.02, "Benchmark systems for network integration of renewable and distributed energy resources," CIGRE International Council on large electric systems, Tech. Rep., July 2009.

[4] IEEE Std 1159-2009, "IEEE recommended practice for monitoring electric power quality," (Revision of IEEE Std 1159-1995), Tech. Rep., June 2009.

[5] M. Karimi, H. Mokhlis, K. Naidu, S. Uddin, and A. A. Bakar, "Photovoltaic penetration issues and impacts in distribution network–A review," *Renewable and Sustainable Energy Reviews*, vol. 53, pp. 594–605, 2016.

[6] A. Navarro-Espinosa and L. F. Ochoa, "Increasing the PV hosting capacity of LV networks: OLTC-fitted transformers vs. reinforcements," in *IEEE PES ISGT*, 2015.

[7] A. Almalaq *et al.*, "Towards increasing hosting capacity of modern power systems through generation and transmission expansion planning," *Sustainability*, vol. 14, no. 5, p. 2998, 2022.

[8] M. S. Aydin, S. W. Alnaser, and S. Z. Althaher, "Using OLTC-fitted distribution transformer to increase residential PV hosting capacity: Decentralized voltage management approach," *Energies*, vol. 15, no. 13, p. 4836, 2022.

[9] X. Xu, J. Li, Z. Xu, J. Zhao, and C. S. Lai, "Enhancing photovoltaic hosting capacity–A stochastic approach to optimal planning of static var compensator devices in distribution networks," *Applied Energy*, vol. 238, pp. 952–962, 2019.

[10] R. Gupta, F. Sossan, and M. Paolone, "Countrywide PV hosting capacity and energy storage requirements for distribution networks: The case of Switzerland," *Applied Energy*, vol. 281, p. 116010, 2021.

[11] J. Seuss, M. J. Reno, R. J. Broderick, and S. Grijalva, "Improving distribution network PV hosting capacity via smart inverter reactive power support," in *IEEE PESGM*, 2015.

[12] F. Ding, B. Mather, and P. Gotseff, "Technologies to increase PV hosting capacity in distribution feeders," in *IEEE PESGM*, 2016.

[13] S. Hashemi and J. Østergaard, "Efficient control of energy storage for increasing the PV hosting capacity of LV grids," *IEEE Transactions on Smart Grid*, vol. 9, no. 3, pp. 2295–2303, 2016.

[14] B. Tavares and F. J. Soares, "An innovative approach for distribution network reinforcement planning: Using DER flexibility to minimize investment under uncertainty," *EPSR*, vol. 183, p. 106272, 2020.

[15] J. M. Home-Ortiz, L. H. Macedo, R. Vargas, R. Romero, J. R. S. Mantovani, and J. P. Catalão, "Increasing RES hosting capacity in distribution networks through closed-loop reconfiguration and Volt/VAr control," *IEEE Trans. Ind. Appl.*, vol. 58, no. 4, pp. 4424–4435, 2022.

[16] D.-L. Schultis, A. Ilo, and C. Schirmer, "Overall performance evaluation of reactive power control strategies in low voltage grids with high prosumer share," *EPSR*, vol. 168, pp. 336–349, 2019.

[17] K. Christakou, "Real-time optimal controls for active distribution networks from concepts to applications," *EPFL Thesis*, p. 212, 2015. [Online]. Available: http://infoscience.epfl.ch/record/214543

[18] R. Luthander, J. Widén, J. Munkhammar, and D. Lingfors, "Self-consumption enhancement and peak shaving of residential photovoltaics using storage and curtailment," *Energy*, vol. 112, pp. 221–231, 2016.

[19] J. Von Appen and M. Braun, "Strategic decision making of distribution network operators and investors in residential photovoltaic battery storage systems," *Applied Energy*, vol. 230, pp. 540–550, 2018.

[20] F. R. S. Sevilla *et al.*, "Techno-economic analysis of battery storage and curtailment in a distribution grid with high PV penetration," *Journal of Energy Storage*, vol. 17, pp. 73–83, 2018.

[21] E. O'Shaughnessy, J. R. Cruce, and K. Xu, "Too much of a good thing? Global trends in the curtailment of solar PV," *Solar Energy*, vol. 208, pp. 1068–1077, 2020.

[22] T. Aziz and N. Ketjoy, "PV penetration limits in low voltage networks and voltage variations," *IEEE Access*, vol. 5, pp. 16 784–16 792, 2017.

[23] T. R. Ricciardi, K. Petrou, J. F. Franco, and L. F. Ochoa, "Defining customer export limits in PV-rich low voltage networks," *IEEE Transactions on Power Systems*, vol. 34, no. 1, pp. 87–97, 2018.

[24] M. Z. Liu, A. T. Procopiou, K. Petrou, L. F. Ochoa, T. Langstaff, J. Harding, and J. Theunissen, "On the fairness of PV curtailment schemes in residential distribution networks," *IEEE Transactions on Smart Grid*, vol. 11, no. 5, pp. 4502–4512, 2020.

[25] M. V. M. Ali, P. Nguyen, W. Kling, A. Chrysochos, T. Papadopoulos, and G. Papagiannis, "Fair power curtailment of distributed renewable energy sources to mitigate overvoltages in low-voltage networks," in *IEEE Eindhoven PowerTech*, 2015.

[26] P. Lusis, L. L. H. Andrew, S. Chakraborty, A. Liebman, and G. Tack, "Reducing the unfairness of coordinated inverter dispatch in PV-rich distribution networks," in *IEEE Milan PowerTech*, 2019.

[27] D. Gebbran, S. Mhanna, Y. Ma, A. C. Chapman, and G. Verbič, "Fair coordination of distributed energy resources with Volt-Var control and PV curtailment," *Applied Energy*, vol. 286, p. 116546, 2021.

[28] Y. Z. Gerdroodbari, R. Razzaghi, and F. Shahnia, "Decentralized control strategy to improve fairness in active power curtailment of PV inverters in low-voltage distribution networks," *IEEE Transactions on Sustainable Energy*, vol. 12, no. 4, pp. 2282–2292, 2021.

[29] Z. Wei, F. De Nijs, J. Li, and H. Wang, "Model-free approach to fair solar PV curtailment using reinforcement learning," in *14th ACM International Conference on Future Energy Systems*, 2023, pp. 14–21.

[30] S. Poudel, M. Mukherjee, R. Sadnan, and A. P. Reiman, "Fairness-aware distributed energy coordination for voltage regulation in power distribution systems," *IEEE Transactions on Sustainable Energy*, 2023.

[31] R. Gupta, P. Buason, and D. K. Molzahn, "Fairness-aware photovoltaic generation limits for voltage regulation in power distribution networks using conservative linear approximations," *8th TPEC*, Feb. 2024.

[32] R. K. Jain, D.-M. W. Chiu, W. R. Hawe *et al.*, "A quantitative measure of fairness and discrimination," *Eastern Research Laboratory, Digital Equipment Corporation, Hudson, MA*, 1984.

[33] A. Kody, A. West, and D. K. Molzahn, "Sharing the load: Considering fairness in de-energization scheduling to mitigate wildfire ignition risk using rolling optimization," in *2022 IEEE 61st Conference on Decision and Control (CDC)*, December 2022.

[34] M. E. Baran and F. F. Wu, "Network reconfiguration in distribution systems for loss reduction and load balancing," *IEEE Transactions on Power Delivery*, vol. 4, no. 2, pp. 1401–1407, 1989.

[35] D. B. Arnold, M. Sankur, R. Dobbe, K. Brady, D. S. Callaway, and A. Von Meier, "Optimal dispatch of reactive power for voltage regulation and balancing in unbalanced distribution systems," in *2016 IEEE Power and Energy Society General Meeting (PESGM)*. IEEE, 2016, pp. 1–5.

[36] R. Gupta, F. Sossan, and M. Paolone, "Grid-aware distributed model predictive control of heterogeneous resources in a distribution network: Theory and experimental validation," *IEEE Transactions on Energy Conversion*, vol. 36, no. 2, pp. 1392–1402, 2020.

[37] J. A. Taylor and F. S. Hover, "Convex models of distribution system reconfiguration," *IEEE Transactions on Power Systems*, vol. 27, no. 3, pp. 1407–1413, 2012.

[38] K. Christakou, J.-Y. LeBoudec, M. Paolone, and D.-C. Tomozei, "Efficient computation of sensitivity coefficients of node voltages and line currents in unbalanced radial electrical distribution networks," *IEEE Transactions on Smart Grid*, vol. 4, no. 2, pp. 741–750, 2013.

[39] L. Bobo, A. Venzke, and S. Chatzivasileiadis, "Second-order cone relaxations of the optimal power flow for active distribution grids: Comparison of methods," *IJEPES*, vol. 127, p. 106625, 2021.

[40] H. Khodr, F. Olsina, P. De Oliveira-De Jesus, and J. Yusta, "Maximum savings approach for location and sizing of capacitors in distribution systems," *EPSR*, vol. 78, no. 7, pp. 1192–1203, 2008.

[41] G. Malmer and L. Thorin, "Network reconfiguration for renewable generation maximization," May 2023, Masters Thesis, Lund University.

[42] J. M. Bright, "Solcast: Validation of a satellite-derived solar irradiance dataset," *Solar Energy*, vol. 189, pp. 435–449, 2019.

[43] W. F. Holmgren, C. W. Hansen, and M. A. Mikofski, "pvlib python: A python package for modeling solar energy systems," *Journal of Open Source Software*, vol. 3, no. 29, p. 884, 2018.

[44] R. Gupta, A. Zecchino, J.-H. Yi, and M. Paolone, "Reliable dispatch of active distribution networks via a two-layer grid-aware model predictive control: Theory and experimental validation," *IEEE Open Access Journal of Power and Energy*, vol. 9, pp. 465–478, 2022.

[45] R. Gupta, F. Sossan, and M. Paolone, "Performance assessment of linearized OPF-based distributed real-time predictive control," in *IEEE Milan PowerTech*, 2019.